Molecular Structures and Photophysical Properties of Dirhodium Fluorophosphine Complexes

Janice Kadis, Yeung-gyo K. Shin, Joel I. Dulebohn, Donald L. Ward, and Daniel G. Nocera*

Department of Chemistry and LASER Laboratory, Michigan State University, East Lansing, Michigan 48824

Received May 9, 1995[⊗]

The excited state properties of a series of singly bonded dirhodium compounds, consisting of Rh^0_2, $Rh^0Rh^{II}X_2$, and $Rh^{II}_2X_4$ (X = Cl and Br) cores coordinated by three bis(difluorophosphino)methylamine ligands, have been investigated. The newly synthesized complexes with X = Br have been structurally characterized. The mixed-valence complex $Rh_2[\mu\text{-}CH_3N(PF_2)_2]_3Br_2[(PF_2)CH_3N(PF_2)]$ crystallizes in the orthorhombic space group $P2_12_12_1$ with $a = 13.868(7)$ Å, $b = 16.090(5)$ Å, $c = 11.614(5)$ Å, $V = 1591(3)$ Å^3, and $Z = 4$; the structure was refined to values of $R = 0.052$ and $R_w = 0.062$. Orange crystals of $Rh_2[\mu\text{-}CH_3N(PF_2)_2]_3Br_4$ are monoclinic with a $C2/c$ space group: $a = 14.62(6)$ Å, $b = 12.20(2)$ Å, $c = 14.33(1)$ Å; $\beta = 106.0(2)°$; $V = 2457(11)$ Å^3; $Z = 4$; and $R = 0.058$ and $R_w = 0.056$. Crystalline solids and low-temperature glasses of each member of the chloride and bromide series exhibit long-lived red luminescence. Excitation profiles and temperature dependencies of the emission bandwidths and lifetimes for all complexes are characteristic of luminescence originating from a dσ* excited state. Efficient nonradiative decay is observed upon the thermal population of an excited state proximate to the lowest energy emissive excited state of these complexes. The nonradiative decay rate constant of the upper excited state is 10^2-10^3 and 10^3-10^4 greater than that of the emissive excited state for complexes with X = Cl and Br, respectively.

Introduction

Atoms held together by a single bond tend to dissociate upon excitation of transitions populating σ* excited states. As early as 1925, the prominent role of photodissociation in the chemistry of inorganic compounds was emerging with Franck's identification of dissociative continua in the absorption spectrum of I_2.[1] Soon thereafter Dymond noted that the intense luminescence of I_2 disappeared upon illumination with light in the continuous region of the absorption spectrum.[2] The spectroscopic studies of Mulliken,[3] and later those of Mathieson and Rees,[4] revealed that these continua were associated with the population of the σ* orbital of the single bond of iodine.

A similar case exists for inorganic compounds featuring metals bound by single bonds. Luminescence from dσ* excited states such as $Mn_2(CO)_{10}$ is circumvented by efficient nonradiative deactivation resulting from the photoinduced cleavage of the metal−metal bond upon dσ* occupation.[5] Although photodissociation can be prevented by spanning M−M cores with bidentate ligands, our recent observations,[6] and those of Miskowski and Stiegman,[7] of luminescence from Pt_2, Rh_2, and Re_2 complexes represent the first reports of long-lived dσ* excited states for M−M compounds. That dσ* luminescence has only recently been observed despite the synthesis of several bridged complexes during the past years underscores the subtle role that electronic factors play in the deactivation of dσ* excited states. Photophysical studies performed by us on singly bonded $LPt^{III}Pt^{III}L$ (L = Cl, Br, and H_2O) tetraphosphates[8] clearly show this to be the case. Time-resolved spectroscopy of these diplatinum complexes reveals a significant temperature dependence of dσ* luminescence arising from the thermal population of an E_u state in the $^3(d\pi^*d\sigma^*)$ manifold, which acquires significant singlet character via a spin−orbit coupling mechanism.

[⊗] Abstract published in *Advance ACS Abstracts,* January 15, 1996.

(1) Franck, J. *Trans. Faraday Soc.* **1925**, *21*, 536.
(2) Dymond, E. G. *Z. Phys.* **1925**, *34*, 553.
(3) (a) Mulliken, R. S. *Phys. Rev.* **1934**, *46*, 549. (b) *Ibid*. **1940**, *57*, 500.
(4) Mathieson, L.; Rees, A. L. G. *J. Chem. Phys.* **1956**, *25*, 753.
(5) (a) Geoffrey, G. L.; Wrighton, M. S. *Organometallic Photochemistry*; Academic Press: New York, 1979. (b) Meyer, T. J.; Caspar, J. V. *Chem. Rev.* **1985**, *85*, 187. (c) Wrighton, M. S.; Graff, J. L.; Luong, J. C.; Reichel, C. L.; Robbins, J. L. In *Reactivity of Metal-Metal Bonds*; Chisholm, M. H., Ed.; ACS Symposium Series 155; American Chemical Society: Washington, DC, 1981; p 85. (d) Rothberg, L. J.; Cooper, N. J.; Peters, K. S.; Vaida, V. *J. Am. Chem. Soc.* **1982**, *104*, 3536. (e) Hepp, A. F.; Wrighton, M. S. *J. Am. Chem. Soc.* **1983**, *105*, 5934. (f) Veillard, A.; Dedieu, A. *Nouv. J. Chim.* **1983**, *7*, 683. (g) Bohling, D. A.; Gill, T. P.; Mann, K. R. *Inorg. Chem.* **1981**, *20*, 194. (h) Wegman, R. W.; Brown, T. L. *Inorg. Chem.* **1983**, *22*, 183. (i) Church, S. P.; Hermann, H.; Grevels, F.-W.; Schaffner, K. *J. Chem. Soc., Chem. Commun.* **1984**, 785. (j) Walker, H. W.; Herrick, R. S.; Olsen, R. J.; Brown, T. L. *Inorg. Chem.* **1984**, *23*, 3748. (k) Reinking, M. K.; Kullburg, M. L.; Cutler, A. R.; Kubiak, C. P. *J. Am. Chem. Soc.* **1985**, *107*, 3517. (l) Seder, T. A.; Church, S. P.; Weitz, E. *J. Am. Chem. Soc.* **1986**, *108*, 7518. (m) Vaida, V. In *High Energy Processes in Organometallic Chemistry*; Suslick, K. S., Ed.; ACS Symposium Series 333; American Chemical Society: Washington, DC, 1987; p 70. (n) Wuu, Y.-M.; Zou, C.; Wrighton, M. S. *J. Am. Chem. Soc.* **1987**, *109*, 5861. (o) Prinslow, D. A.; Vaida, V. *J. Am. Chem. Soc.* **1987**, *109*, 5097. (p) Yasukufu, K.; Hiraga, N.; Ichimura, K.; Kobayashi, T. In *Photochemistry and Photophysics of Coordination Compounds*; Yersin, H., Vogler, A., Eds.; Springer-Verlag: New York, 1987; p 271. (q) Stufkens, D. J. In *Stereochemistry of Organometallic and Inorganic Compounds*; Bernal, I., Ed.; Elsevier: Amsterdam, 1989; Vol. 3, p 226. (r) Turner, J. J.; Poliakoff, M.; Healy, M. A. *Pure Appl. Chem.* **1989**, *61*, 787. (s) Stufkens, D. *Coord. Chem. Rev.* **1990**, *104*, 39. (t) Sykora, J.; Sima, J. *Coord. Chem. Rev.* **1990**, *107*, 88. (u) Lemke, F. R.; Granger, R. M.; Morgenstern, D. A.; Kubiak, C. P. *J. Am. Chem. Soc.* **1990**, *112*, 4052. (v) Tenhaeff, S. C.; Tyler, D. R. *Organometallics* **1991**, *10*, 1116. (w) Dixon, A. J.; George, M. W.; Hughes, C.; Poliakoff, M.; Turner, J. J. *J. Am. Chem. Soc.* **1992**, *114*, 1719.
(6) Dulebohn, J. I.; Ward, D. L.; Nocera, D. G. *J. Am. Chem. Soc.* **1988**, *110*, 4054.
(7) (a) Stiegman, A. E.; Miskowski, V. M. *J. Am. Chem. Soc.* **1988**, *110*, 4053. (b) Stiegman, A. E.; Miskowski, V. M.; Gray, H. B. *J. Am. Chem. Soc.* **1986**, *108*, 2781.
(8) Shin, Y.-g. K.; Miskowski, V. M.; Nocera, D. G. *Inorg. Chem.* **1990,** *29*, 2308.

0020-1669/96/1335-0811$12.00/0

Our interest in further elaborating the mechanisms governing dσ* luminescence is stimulated with our recent synthesis of the related series of dirhodium bis(difluorophosphino)methylamine ($CH_3N(PF_2)_2$, dfpma) compounds $Rh_2(dfpma)_3(PF_3)_2$, $Rh_2(dfpma)_3Cl_2(PF_3)$, and $Rh_2(dfpma)_3Cl_4$.[9] Luminescence, observed for this series of compounds, is associated with the singly bonded $Rh^0Rh^{II}Cl_2$ and $Rh^{II}_2Cl_4$ cores. We now report the synthesis and characterization of the parallel bromide series. Whereas the chloride and bromide complexes of $Rh_2(dfpma)_3X_4$ are structurally analogous, the PF_3 bound axially to the Rh(0) center in $Rh_2(dfpma)_3Cl_2(PF_3)$ is replaced by a dfpma ligand in the bromide compound to give $Rh_2(dfpma)_3Br_2(\eta^1$-dfpma). Absorption spectra not only suggest chloride and bromide congeners to be electronically similar but also the Rh^0_2, $Rh^0Rh^{II}X_2$, and $Rh^{II}_2X_4$ series to be analogous despite the different d-electron counts of the bimetallic cores. We show that the long-lived luminescence from this series of fluorophosphine compounds most likely originates from a dπ*dσ* excited state, and possible models rationalizing the observed photophysics for the Rh_2 series are discussed.

Experimental Section

Synthesis of Dirhodium Fluorophosphine Complexes. All synthetic manipulations, filtrations, and recrystallizations were performed under a purified argon atmosphere. The $Rh_2(dfpma)_3(PF_3)_2$, $Rh_2(dfpma)_3Cl_2(PF_3)$, and $Rh_2(dfpma)_3Cl_4$ complexes were synthesized by previously described methods.[9] For the corresponding bromide derivatives, $[RhBr(PF_3)_2]_2$ was the starting material, which was obtained by reacting $[RhCl(PF_3)_2]_2$ with excess NaBr.[10] Addition of $CH_3N(PF_2)_2$ (0.50 mL, 4.3 mmol) to $[RhBr(PF_3)_2]_2$ (0.13 g, 0.184 mmol) in 15 mL of benzene followed by 9 h of heating at reflux temperature gave the red-orange precipitate of the $Rh^0Rh^{II}Br_2$ compound, which was collected by filtration, washed with benzene, and dried under vacuum. For the $Rh^{II}_2Br_4$ derivative, $CH_3N(PF_2)_2$ (0.2 mL, 1.73 mmol) was added via syringe to a benzene solution of $[RhBr(PF_3)_2]_2$. This reaction mixture was charged with bromine (0.02 mL, 0.390 mmol), and the solution was heated at reflux temperature for 3.5 h. The solvent volume was reduced by two-thirds under an argon flow, and hexane (6 mL) was added to promote precipitation. The ensuing precipitate was filtered and dried under vacuum. Crystals of $Rh_2(dfpma)_3Br_2(\eta^1$-dfpma) and $Rh_2(dfpma)_3Br_4$ were obtained by layering CH_2Cl_2 solutions of the compounds with hexane. The compounds were identified by FABMS and X-ray crystallographic analysis.

X-ray Crystallography. The diffraction data for the dirhodium complexes were collected on a Rigaku AFC6S diffractometer using graphite monochromated Mo Kα (λ = 0.71069 A) radiation and a 2 KW sealed tube generator. The intensity data were collected by using $\omega - 2\theta$ scans at a rate of 4.0/min (in ω; three rescans) for $Rh_2(dfpma)_3Br_2(\eta^1$-dfpma) and 16.0/min (in ω; two rescans) for $Rh_2(dfpma)_3Br_4$. Calculations were performed on a VAX 11/750 computer using the TEXSAN crystallographic software package provided by Molecular Structure Corp. Crystal parameters and details of intensity collection and refinement for the structure determinations of $Rh_2(dfpma)_3Br_2(\eta^1$-dfpma) and $Rh_2(dfpma)_3X_4$ are listed in Table 1. Complete tables of positional parameters, bond distances, bond angles, anisotropic thermal parameters, and hydrogen atom parameters are available as Supporting Information.

$Rh_2[\mu$-$CH_3N(PF_2)_2]_3Br_2[(PF_2)CH_3N(PF_2)]$ (1). A deep maroon irregular crystal of **1** (approximate dimensions, 0.14 × 0.20 × 0.30 mm) was mounted at the end of a glass fiber and coated with N-Paratone oil. The cell parameters and an orientation matrix were obtained from a least-squares refinement of 25 reflections in the range $15.50 < 2\theta < 19.21$. The space group was found to be $P2_12_12_1$.

A total of 2614 reflections were collected at a temperature of −90 ± 3 °C. The structure was solved by direct methods. The non-hydrogen atoms were refined anisotropically. The final cycle of full-matrix least-squares refinement was based on 1748 observed reflections ($I > 3.00\sigma$(I)) and 320 variable parameters and converged (largest parameter shift was 0.11 times its esd) with unweighted and weighted agreement factors of 0.052 and 0.062, respectively. The largest peak in the final difference map was 1.12 e/Å^3.

Table 1. Crystallographic Data for $Rh_2(dfpma)_3Br_2(\eta^1$-dfpma) (**1**) and $Rh_2(dfpma)_3X_4$ (**2**)

	1	2
chemical formula	$Rh_2F_{16}Br_2P_8N_4C_4H_{12}$	$Rh_2F_{12}Br_4P_6N_3C_3H_9$
formula weight	1033.55	1026.37
space group	$P2_12_12_1$ (19)	$C2/c$(15)
a (Å)	13.868(7)	14.62(6)
b (Å)	16.090(5)	12.20(2)
c (Å)	11.614(5)	14.33(1)
α (deg)	90	90
β (deg)	90	106.0(2)
γ (deg)	90	90
V (Å^3)	1591(3)	2457(11)
Z	4	4
T (°C)	−90	23
λ (Mo Kα) (Å)	0.71069	0.71069
ρ_{calcd} (g cm^{-3})	2.649	2.775
μ (cm^{-1})	49.17	21.5
$R(F_o)^a$	0.052	0.058
$R_w(F_o)^b$	0.062	0.056

^{a} $R = \sum||F_o| - |F_c||/\sum|F_o|$. ^{b} $R_w = [\sum w(|F_o| - |F_c|)^2/\sum w|F_o|^2]^{1/2}$; $w = 1/(\sigma^2|F_o|)$.

$Rh_2[CH_3N(PF_2)_2]_3Br_4$ (2). An orange irregular crystal of **2** (approximate dimensions, 0.08 × 0.12 × 0.20 mm) was mounted on a glass fiber. The cell parameters and an orientation matrix were obtained from a least-squares refinement using the setting angles of six carefully centered reflections in the range $20.48 < 2\theta < 22.61$ corresponding to a monoclinic cell. The space group was determined to be $C2/c$.

The data were collected at a temperature of 23 ± 1 °C; a total of 2389 reflections were collected, of which 2279 were unique. The intensities of three representative reflections, which were measured after every 150 reflections, declined by 0.080%. A linear correction factor was applied to the data to account for this phenomenon. The structure was solved by direct methods. The non-hydrogen atoms were refined either anisotropically or isotropically. The final cycle of full-matrix least-squares refinement was based on 729 observed reflections ($I > 3.00\sigma$(I)) and converged (largest parameter shift was 0.01 times its esd) with weighted and unweighted agreement factors of 0.058 and 0.056, respectively. The largest peak in the final difference map was 1.09 e/A^3.

Spectroscopic Measurements. Electronic absorption spectra were recorded on either a Cary 17 or a Varian 2300 Uv−vis−near-IR spectrometer. Dried CH_2Cl_2 was employed as solvent and deoxygenated by vigorously bubbling argon. Molar absorptivities were obtained from plots of at least four experimental points. Time-resolved and steady state luminescence spectra were recorded with a Nd:YAG pulsed-laser system (λ_{exc} = 355 nm, fwhm = 8 ns)[11] and a high-resolution emission spectrometer (λ_{exc} = 365 nm)[12] constructed at Michigan State University. Variable temperature luminescence and lifetime measurements were recorded on crystalline samples cooled with an Air Products closed-cycle cryogenic system by methods described elsewhere.[8] Excitation spectra of the dirhodium complexes were recorded on the high-resolution emission spectrometer with the following modifications: a quartz beam splitter was placed in the excitation optical path to direct a portion of the excitation light from a 150 W Xe lamp to a photodiode, which was used to monitor the intensity profile of the excitation source thereby permitting the excitation intensity to be normalized; the phase-modulated intensities of the excitation and emission light were detected with individual lock-in amplifiers; and the outputs of the lock-in amplifiers and the photodiode were fed to a microcomputer, which permitted the emission intensity to be simultaneously corrected for excitation intensity and photodiode responses.

(9) Dulebohn, J. I.; Ward, D. L.; Nocera, D. G. *J. Am. Chem. Soc.* **1990**, *112*, 2969.
(10) Bennett, M. A.; Patmore, D. J. *Inorg. Chem.* **1971**, *10*, 2387.
(11) Newsham, M. D.; Giannelis, E. P.; Pinnavaia, T. J.; Nocera, D. G. *J. Am. Chem. Soc.* **1988**, *110*, 3885.
(12) Mussell, R. D.; Nocera, D. G. *J. Am. Chem. Soc.* **1988**, *110*, 2764.

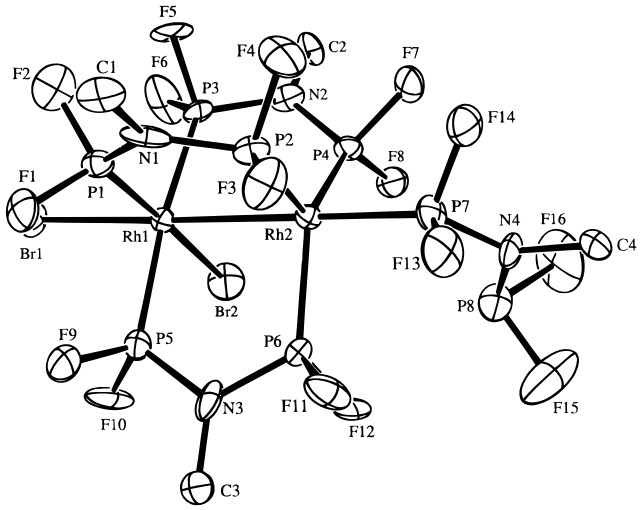

Figure 1. ORTEP drawing and numbering scheme of $Rh_2(dfpma)_3Br_2(\eta^1\text{-dfpma})$ (**1**) with 50% probability ellipsoids.

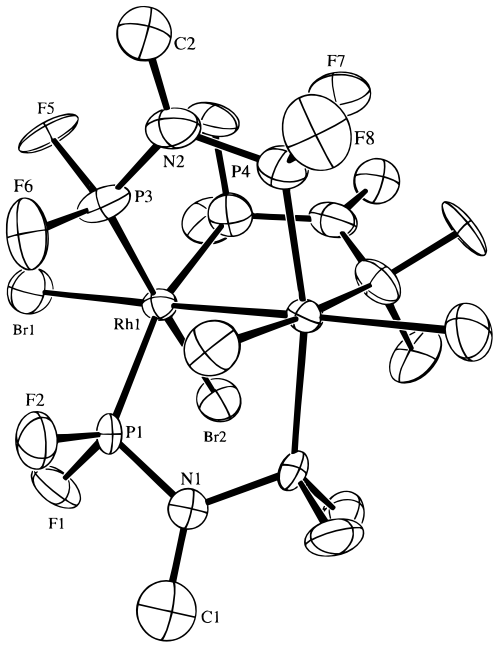

Figure 2. ORTEP view of $Rh_2(dfpma)_3Br_4$ (**2**) showing the numbering scheme. Thermal parameters are shown at the 50% level.

Samples employed for measurements were in crystalline or powder form in EPR tubes that were immersed in liquid nitrogen in a finger Dewar flask. A 715-nm cutoff filter was installed in front of the emission monochromator, and slit widths were 5 mm/5 mm (1.8 nm/mm) and 3 mm/3 mm (1.6 nm/mm) for excitation and emission monochromators, respectively.

Results and Discussion

Compounds **1** and **2** are obtained from the symmetric Rh^I_2 complex $[RhBr(PF_3)_2]_2$. The formation of **1** proceeds smoothly in the presence of bis(difluorophosphino)methylamine to yield the $Rh^0Rh^{II}Br_2$ core ligated by three bridging fluorophosphine ligands. Similar to our observations for the analogous chloride complexes, the reaction corresponds to an intramolecular disproportionation of the Rh^I_2 starting material. When Br_2 is introduced to the Rh^I_2 complex in the presence of the bidentate fluorophosphine, the two-electron mixed-valence compound is not stable and the fully oxidized $Rh^{II}_2Br_4$ core is obtained.

The ORTEP diagrams of $Rh_2(dfpma)_3Br_2(\eta^1\text{-dfpma})$ and $Rh_2(dfpma)_3Br_4$ are shown in Figures 1 and 2. The structural features observed for the $Rh^0Rh^{II}Cl_2$ and $Rh^{II}_2Cl_4$ cores are retained in these complexes with trigonal bipyramidal geometry observed about the Rh(0) center and a pseudooctahedral coordination sphere surrounding the Rh(II) center. Whereas the chloro and bromo $Rh_2(dfpma)_3X_4$ complexes are structurally analogous, the $Rh_2(dfpma)_3Br_2(\eta^1\text{-dfpma})$ compound features monodentate coordination of a dfpma ligand in place of the axial PF_3 in the $Rh_2(dfpma)_3Cl_2(PF_3)$ complex. Preference for axial coordination of only one phosphorus of the dfpma ligand as opposed to coordination of a small molecule π-accepting ligand such as PF_3 has been observed previously in the reaction of $Co_2(CO)_8$ with dfpma to yield $Co_2(dfmpa)_3(\eta^1\text{-dfmpa})_2$.[13] The electronic properties of the $Rh^0Rh^{II}X_2$ core (*vide infra*) do not appear to be greatly perturbed whether PF_3 or dfpma occupies the axial coordination site of the Rh(0) center.

Table 2. Selected Bond Distances (Å) and Bond Angles (deg) of the Rh^0_2, $Rh^0Rh^{II}X_2$, and $Rh^{II}_2X_4$ Cores of the Binuclear Fluorophosphine Compounds

	$Rh_2(dfpma)_3(PF_3)_2$	$Rh_2(dfpma)_3X_2(L)$		$Rh_2(dfpma)_3X_4$	
		X = Cl	X = Br	X = Cl	X = Br
		Bond Distance			
d(Rh−Rh)	2.841(2)	2.785(1)	2.798(2)	2.707(1)	2.750(8)
$d(Rh-X)_{ax}$		2.431(2)	2.579(3)	2.416(2)	2.555(6)
$d(Rh-X)_{eq}$		2.385(2)	2.524(4)	2.392(2)	2.519(9)
		Bond Angle			
Rh−Rh−X1		176.46(6)	177.1(1)	175.75(5)	173.9(2)
X1−Rh−X2		92.81(7)	92.9(1)	90.69(8)	89.9(3)

The primary structural differences between the chloro and bromo analogs of the $Rh_2(dfpma)_3X_2(L)$ (L = PF_3 or dfpma) and $Rh_2(dfpma)_3X_4$ complexes occur in the $Rh^0Rh^{II}X_2$ and $Rh^{II}_2X_4$ cores. Table 2 displays selected bond distances and angles for the two classes of compounds; the appropriate data for the Rh^0_2 complex are also included. The dirhodium complexes display bond lengths characteristic of Rh−Rh single bonds,[14] which arise from the pairing of an odd electron residing in the d_{z^2} orbital of a d^9 Rh^0P_4 fragment or d^7 $Rh^{II}P_3X_2$ fragment to yield species with d-electron configurations of $(d^8)d^1-d^1-(d^8)$, $(d^8)d^1-d^1(d^6)$, and $(d^6)d^1-d^1(d^6)$ (for the Rh^0_2, $Rh^0Rh^{II}X_2$, and $Rh^{II}_2X_4$ cores, respectively).[9] The increase in Rh−Rh bond length along the chloride and bromide series Rh^{II}_2 < Rh^0Rh^{II} < Rh^0_2 is expected in view of the larger atomic radius of Rh-(0) as compared to Rh(II). Along similar lines, the increase of ~0.14 Å in the axial and equatorial Rh−X bond distances upon replacement of chloride with bromide for $Rh_2(dfpma)_3X_4$ and $Rh_2(dfpma)_3X_2(L)$ is consistent with the larger atomic radius of the bromine atom (r(Br) in Br_2 = 1.141 Å, r(Cl) in Cl_2 = 0.994 Å, Δr = 0.147 Å[15]). The Rh−Rh separation of a given complex is also larger when X = Br. These trends in Rh−Rh and Rh−X distances are observed for other binuclear rhodium compounds, including $Rh_2X_6(dppm)_2$[16] where the Rh−Rh bond length increases by 0.102 Å and the average Rh−X bond length increases by 0.131 Å upon the substitution of Br for Cl.

The electronic absorption spectrum of $Rh_2(dfpma)_3(PF_3)_2$, shown in Figure 3, provides a benchmark for interpreting the

(13) King, R. B.; Chang, M.; Newton, M. G. *J. Organomet. Chem.* **1985**, *296*, 15.
(14) (a) Jenkins, J. A.; Ennett, J. P.; Cowie, M. *Organometallics* **1988**, *7*, 1845. (b) Cotton, F. A.; Eagle, C. T.; Price, A. C. *Inorg. Chem.* **1988**, *27*, 4362. (c) Cotton, F. A.; Dunbar, K. R.; Verbruggen, M. G. *J. Am. Chem. Soc.* **1987**, *109*, 5498. (d) Balch, A. L.; Oram, D. E. *J. Organomet. Chem.* **1988**, *349*, 245. (e) Cowie, M.; Dickson, R. S. *Inorg. Chem.* **1981**, *20*, 2682. (f) Cowie, M.; Dwight, S. K. *Inorg. Chem.* **1980**, *19*, 2508. (g) Cowie, M. *Inorg. Chem.* **1979**, *18*, 286.
(15) Douglas, B. E.; McDaniel, D. H.; Alexander, J. J. *Concepts and Models of Inorganic Chemistry*, 2nd ed.; Wiley: New York, 1983; p 581.
(16) Cotton, F. A.; Dunbar, K. R.; Eagle, C. T.; Falvello, L. R.; Price, A. C. *Inorg. Chem.* **1989**, *28*, 1754.

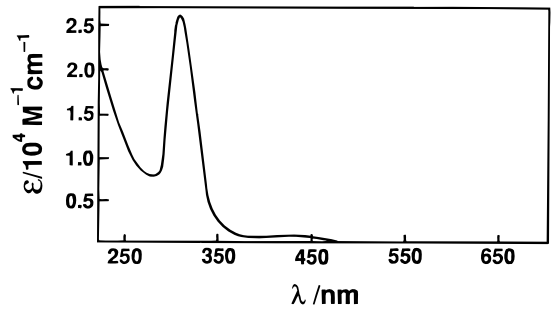

Figure 3. Electronic absorption spectrum of $Rh_2(dfpma)_3(PF_3)_2$ dissolved in CH_2Cl_2 at room temperature.

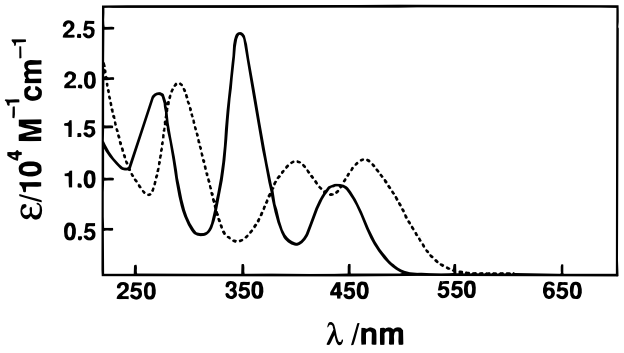

Figure 4. Electronic absorption spectrum of $Rh_2(dfpma)_3Cl_4$ (—) and $Rh_2(dfpma)_3Br_4$ (– – –) in CH_2Cl_2 at room temperature.

electronic absorption spectra of this series of singly bonded metal−metal compounds. The absorption spectrum is typical of M−M compounds[17] with an intense 305-nm band attributable to the allowed $d\sigma \rightarrow d\sigma^*$ transition and the less intense band at 440 nm consistent with $d\pi^* \rightarrow d\sigma^*$ promotion. The high optical electronegativity of the terminal PF_3 ligand reduces configurational mixing of the $d\sigma$ and $L\sigma$ orbitals, which is observed when more easily ionizable ligands such as halides or pseudohalides are coordinated axially to a M−M core.[17,18] Accordingly, the importance of configurational mixing of $L\sigma$ and $d\sigma$ orbitals for the dirhodium fluorophosphines is apparent upon comparison of the spectra of $Rh_2(dfpma)_3X_4$ and $Rh_2(dfpma)_3X_2(L)$ (X = Cl and Br) to that of $Rh_2(dfpma)_3(PF_3)_2$.

The absorption profiles of the d^7-d^7 dimers $Rh_2(dfpma)_3Cl_4$ and $Rh_2(dfpma)_3Br_4$ (Figure 4) are more congested in the Uv spectral region than that of $Rh_2(dfpma)_3(PF_3)_2$. Though the Rh−Rh separation differs by no more than 0.15 Å in this set of complexes, no absorption comparable in energy to the 305-nm $d\sigma \rightarrow d\sigma^*$ transition of $Rh^0{}_2$ complex is observed. However, intense transitions to higher and lower energy of the $Rh^0{}_2$ $d\sigma \rightarrow d\sigma^*$ absorption are present (λ_{max}/nm (ϵ/$M^{-1}cm^{-1}$) = 265 (18 700) and 335 (23 000) for $Rh_2(dfpma)_3Cl_4$; λ_{max}/nm (ϵ/M^{-1} cm^{-1}) = 289 (19 600) and 398 (11 400) for $Rh_2(dfpma)_3Br_4$). Notably, these transitions exhibit a ~3500 cm^{-1} red shift with the replacement of chloride by bromide. In contrast, the energy of the lowest energy band is much less sensitive to halide substitution (λ_{max}/nm (ϵ/M^{-1} cm^{-1}) = 445 (9430) for $Rh_2(dfpma)_3Cl_4$; λ_{max}/nm (ϵ/M^{-1} cm^{-1}) = 462 (11 700) for $Rh_2(dfpma)_3Br_4$). This trend is also observed in the absorption spectra of the $Rh^0Rh^{II}X_2$ compounds (Figure 5). Absorption profiles show bands in energy regions similar to $Rh^{II}{}_2X_4$, and a red shift is observed upon bromide substitution. This result is

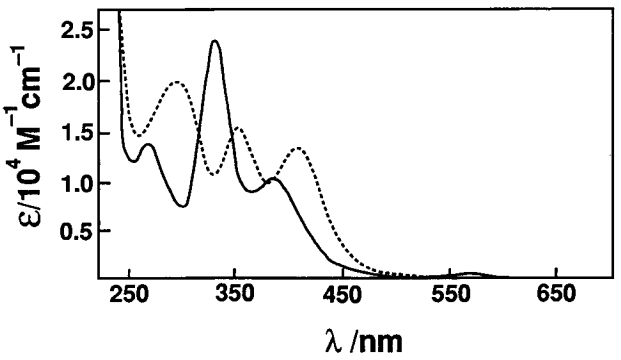

Figure 5. Electronic absorption spectrum of $Rh_2(dfpma)_3Cl_2(PF_3)$ (—) and $Rh_2(dfpma)_3(\eta^1\text{-dfpma})Br_2$ (– – –) in CH_2Cl_2 at room temperature.

not surprising in view of the similarities of the frontier molecular orbitals of the d^7-d^7 and d^7-d^9 dirhodium compounds.[9]

These spectral trends of the dirhodium fluorophosphine series are comparable to those of the d^7-d^7 $Rh_2TMB_4L_2{}^{n+}$ compounds (TMB = 2,5-dimethyl-2,5-diisocyanohexane; L = H_2O, CH_3CN (n = 4); L = Cl, Br (n = 2)). In the cases of L = H_2O or CH_3CN, a single intense absorption is observed at 308 nm and assigned to $d\sigma \rightarrow d\sigma^*$.[18] The considerable red shift of the $d\sigma \rightarrow d\sigma^*$ transition upon substitution of L by axial chloride and further red-shift with bromide (~2200 cm^{-1} as compared to our observation of ~3500 cm^{-1} for the fluorophosphines) is attributed to extensive mixing of the metal $d\sigma$ orbital with the axial $X\sigma$ orbitals of the halide-substituted compounds. As expected from a configurational interaction scheme, the ligand-to-metal charge transfer transition, $X\sigma \rightarrow d\sigma^*$, appears to higher energy of the $d\sigma \rightarrow d\sigma^*$ transition. The lowest energy $d\pi^* \rightarrow d\sigma^*$ transition shows only a moderate halide dependence, red shifting only slightly along a halide series.

Despite similarities in the energy of the spectral profile of $Rh_2(dfpma)_3X_2(L)$ and $Rh_2(dfpma)_3X_4$ to other M−M dimers, there are notable differences. For a typical M−M compound, the spectrum is dominated by $d\sigma \rightarrow d\sigma^*$ and the higher energy configurationally mixed $X\sigma \rightarrow d\sigma^*$ bands exhibit weaker intensity; the weakest transition is usually $d\pi^* \rightarrow d\sigma^*$. Conversely, the intensities of the three bands in the absorption manifold of the $Rh_2(dfpma)_3X_2(L)$ and $Rh_2(dfpma)_3X_4$ complexes are similar. Undoubtedly this result is due in large part to the lower molecular symmetry of the dirhodium complexes as compared to the D_{4h} symmetry of many M−M dimers reported to date. In these lower symmetry molecules, configuration interaction between metal- and ligand-based orbitals will be more extensive. Hence it is difficult to quantitatively correlate the transitions arising from $d\pi$ and $d\delta$ orbital symmetries in D_{4h} dimers with those of the $Rh_2(dfpma)_3X_2(L)$ and $Rh_2(dfpma)_3X_4$ compounds. Thus definitive assignments for the dirhodium fluorophosphine series based on the spectral trends of higher symmetry D_{4h} M−M complexes are tenuous. Nonetheless, the band shapes and energy trends of the absorption profile observed in this dirhodium series are consistent with transitions involving the promotion of an electron from configurationally mixed $L\sigma$ and $d\sigma$ orbitals to $d\sigma^*$ and with a low-energy transition manifold of $d\pi^* \rightarrow d\sigma^*$ parentage.

The luminescence properties of the dirhodium compounds further support an electronic structure dominated by M−M parentage. Table 3 lists the luminescence band energy maxima and emission lifetimes (T = 77 K). The luminescence spectral features are commensurate with the emerging characteristics of $d\sigma^*$ luminescence.[6−8] The full-width at half-height of the emission bands exhibits a substantial temperature sensitivity, increasing by more than 1500 cm^{-1} from 10 K to the highest temperatures at which emission can be detected for each

(17) Miskowski, V. M.; Gray, H. B. In *Understanding Molecular Properties*; Avery, J.; Dahl, J. P.; Hansen, A. E., Eds.; Reidel: Dordrecht, 1987; p 1.
(18) Miskowski, V. M.; Smith, T. P.; Loehr, T. M.; Gray, H. B. *J. Am. Chem. Soc.* **1985**, *107*, 7925.

Table 3. Photophysical Properties of Dirhodium Fluorophosphine Complexes

compound	$\lambda_{em,max}$ (nm)[a]	τ (μs)[b]	ΔE (cm^{-1})[c]	k_0 (s^{-1})[c]	k_1 (s^{-1})[c]
$Rh_2(dfpma)_3(PF_3)_2$	805	74	369	1.1×10^4	1.1×10^6
$Rh_2(dfpma)_3Cl_2(PF_3)_2$	810	270	425	2.0×10^3	3.7×10^5
$Rh_2(dfpma)_3Br_2(\eta^1\text{-dfpma})$	760	190	595	5.4×10^3	2.2×10^6
$Rh_2(dfpma)_3Cl_4$	820	300	463	3.0×10^3	3.5×10^5
$Rh_2(dfpma)_3Br_4$	850	79	895	1.3×10^4	1.6×10^8

[a] Emission maximum of CH_2Cl_2 solutions at 77 K. [b] Lifetime of solid samples at 77 K. [c] Obtained from best fit of temperature dependence of the observed emission decay rate constants to either eq 1 or 2.

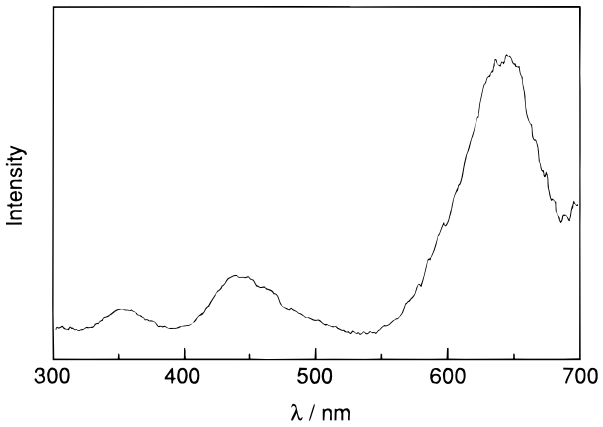

Figure 6. Unpolarized excitation spectra of crystalline $Rh_2(dfpma)_3Cl_2(PF_3)$ at 77 K.

complex. Moreover, luminescence is not detected from solutions at temperatures equivalent to those at which the crystalline solids emit.

Several data suggest that the state parentage of the dσ* luminescence is the promotion of an electron from the (dπ*,dσ*) manifold that is triplet paired. First, the nature of the halide affects the emission energy only marginally across the series. This energy insensitivity is consistent with the expectation of only small configurational mixing of the dσ* orbital (owing to the large energy gap between Lσ and dσ* orbitals) and, as observed in absorption spectra, with the slight energy dependence of the lowest energy absorption manifold. Second, excitation spectra of the dirhodium series are consistent with emission arising from the spin forbidden states of this lowest energy manifold. The excitation spectrum for $Rh_2(dfpma)_3Cl_2(PF_3)$, shown in Figure 6, is representative of the dirhodium series. Three excitation bands are observed, and irradiation at wavelengths coincident with the maxima of these three bands produces the emission spectrum of $Rh_2(dfpma)_3Cl_2(PF_3)$. Whereas peaks energetically coincident with absorptions in the high-energy absorption manifold of $Rh_2(dfpma)_3Cl_2(PF_3)$ are present, the spectrum exhibits an additional feature to lower energy. For each dirhodium compound, the tail of this low-energy excitation band overlaps the higher energy tail of the emission profile. As suggested for the $LPt^{III}Pt^{III}L$ tetraphosphates, such low-energy features are consistent with transitions arising from a ^{3}(dπ*dσ*) spin−orbit manifold, and it is this state from which the observed luminescence arises.

The luminescence from each of the bimetallic complexes decays monoexponentially. Figures 7−9 depict the temperature dependencies of the observed lifetimes for the Rh^0_2, $Rh^0Rh^{II}X_2$, and $Rh^{II}_2X_4$ fluorophosphines, respectively. The lifetimes exhibit a temperature independent regime followed by a monotonic decrease with increasing temperatures. Paralleling

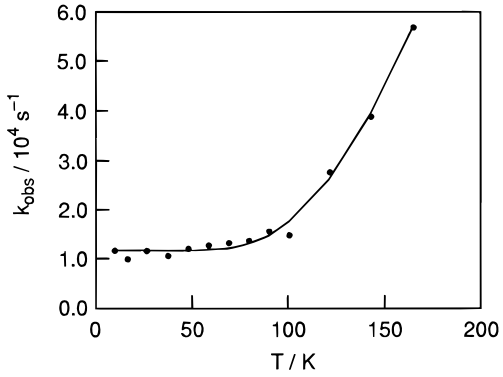

Figure 7. Plot of the temperature dependence of the observed emission decay constant for a solid sample of $Rh_2(dfpma)_3(PF_3)_2$. The solid line is the fit of the data to eq 2.

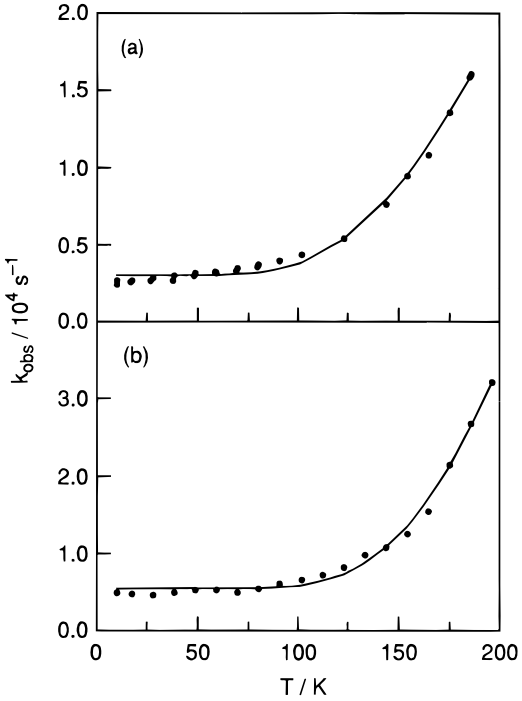

Figure 8. Plot of the observed emission decay constant from solid samples of (a) $Rh_2(dfpma)_3Cl_2(PF_3)$ and (b) $Rh_2(dfpma)_3Br_2(\eta^1\text{-dfpma})$ vs temperature and a fit of these data (solid line) to eq 2.

this decrease in lifetime is a concomitant decrease in luminescence intensity arising from the introduction of an efficient nonradiative decay pathway with increasing temperature (see below). Thus lifetimes could be measured only up to temperatures at which luminescence could be detected with our instrumentation.

The temperature dependence of the excited state lifetimes may be described by thermally activated decay from the excited state

$$k_{obs} = k_0 + k_1 \exp(-\Delta E_a/k_B T) \quad (1)$$

Alternatively the observed rate constant for decay from a higher energy excited state in thermal equilibrium with the emitting state is given by[8,19]

$$k_{obs} = \frac{k_0 + k_1 \exp(-\Delta E/k_B T)}{1 + \exp(-\Delta E/k_B T)} \quad (2)$$

The latter is a Boltzmann-averaged decay rate constant and differs from eq 1 by the normalization term in the denominator.

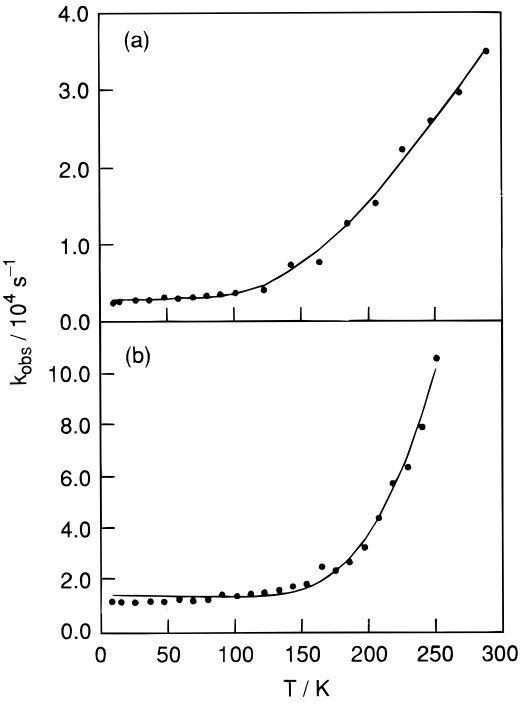

Figure 9. Plot of the observed emission decay constant from solid samples of (a) $Rh_2(dfpma)_3Cl_4$ and (b) $Rh_2(dfpma)_3Br_4$ vs temperature and a fit of these data (solid line) to eq 2.

As has been discussed previously,[19b] the appropriate expression depends upon the number of low-lying states and their degeneracies with eqs 1 and 2 yielding the same results when $\Delta E \geq 3k_BT$. This is the case here for all complexes, and consequently, the fits of the observed rate constants to the activated and Boltzmann-averaged models yield virtually identical results. Calculated rate constants and energy gaps for the dirhodium series are summarized in Table 3 where k_0 and k_1 are the decay constants for emitting and deactivating excited states, respectively, and ΔE is the energy gap between these states. We have chosen to show the best fits of our data to eq 2 in Figures 7−9. The experimentally determined decay constant of the higher energy, thermally accessible excited state is 10^2-10^3 greater than that of the lowest energy state. Additionally, the calculated energy gap monotonically increases with increased halide substitution ($\Delta E(Rh^0{}_2) < \Delta E(Rh^0Rh^{II}X_2) < \Delta E(Rh^{II}{}_2X_4)$). For a given complex, the energy gaps of the bromide derivative are larger than that for its chloride counterpart, as is the decay constant from the upper excited state relative to the lowest energy excited state ($k_1/k_0 \sim 10^3-10^4$ for bromide compounds, as compared to only 10^2 for the chloride complexes).

The observed photophysics of the dirhodium series may be due to the thermal population of a state within the spin−orbit manifold of the $d\pi^*d\sigma^*$ configuration. Such a mechanism has been invoked by us to explain the photophysical properties of singly bonded $LPt^{III}Pt^{III}L$ tetraphosphates,[8] and it is also consistent with the observations by Miskowski et al. for the $LPt^{III}Pt^{III}L$ tetrasulfates.[20] We have shown that the photophysical properties of the tetraphosphates are consistent with luminescence originating from a spin−orbit excited state that is predicted to be nearly pure triplet in character.[8] The temperature dependence of the lifetime arises from the thermal population of the $E_u(^3E_u)$ state in the $^3(d\pi^*d\sigma^*)$ manifold, which acquires significant singlet character from its energetically proximate singlet counterpart $E_u(^1E_u)$.[21] For the dirhodium fluorophosphine series, this model is preserved rigorously only for $Rh_2(dfpma)_3(PF_3)_2$. In the D_3 point group, the lowest energy excited state pair ($A_1(^3E')$, $A_2(^3E')$) of the $^3(d\pi^*d\sigma^*)$ manifold remains unique and proximate to the higher energy $E(^3E')$ state, which may mix with the $E(^1E')$ state of the $^1(d\pi^*d\sigma^*)$ configuration. Accordingly, as observed for the for $LPt^{III}Pt^{III}L$ tetraphosphates and sulfates, the luminescence properties of $Rh_2(dfpma)_3(PF_3)_2$ may be explained by a two-state Boltzmann model, where the upper excited state provides a facile decay pathway to the ground state. However, the lowest energy states of the $^3(d\pi^*d\sigma^*)$ manifold do not remain unique from the states of the $^1(d\pi^*d\sigma^*)$ manifold upon descent in symmetry to the C_s and C_2 molecular point groups of the $Rh_2(dfpma)_3X_2(L)$ and $Rh_2(dfpma)_3X_4$ compounds, respectively. Thus for a spin−orbit coupling mechanism to be preserved, the electronic structure of these compounds would have to reflect the pseudooctahedral and trigonal bipyramidal parentage of the rhodium group fragments. In support of a spin−orbit mechanism, we note that the energy gaps and the nonradiative decay constants are increased as the axial ligand is changed along the series $PF_3 < Cl < Br$, as was observed along a similar series for the Pt_2 tetraphosphates. In addition, first-order spin−orbit considerations also predict that the ΔE's of the Rh_2 series should be approximately one-half that of the Pt_2 series. Except for $Rh^{II}{}_2Br_4$ which is comparable to $BrPt^{III}Pt^{III}Br$ tetraphosphate, the Rh_2 series exhibits smaller energy gaps than the Pt_2 tetraphosphates.[22] The values of ΔE for the $Rh^0{}_2$ and $Rh^0Rh^{II}Br_2$ complexes are ∼70% that of the bromo and aquo complexes of Pt_2 tetraphosphate, respectively, and those of $Rh^0Rh^{II}Cl_2$ and $Rh^{II}{}_2Cl_4$ are ∼45% that of the chloro complex of Pt_2 tetraphosphate.

Alternatively, the Rh_2 dfmpa series is distinguished from the Pt_2 complexes inasmuch as the bridging ligands are twisted significantly thereby allowing for considerable distortion along the metal−metal bond. Rotation about the metal−metal bond may provide an efficient decay pathway to ground state. In this case, ΔE is the activation energy for rotation. Similar arguments have been invoked for the nonradiative decay of twisted ethylene, where rotation about the olefin bond leads to prompt crossover to ground state.[23] In ethylene, the $^1\pi\pi^*$ excited state is stabilized with rotation owing to loss of the π-bond, and efficient radiationless decay occurs at the minimum. Although the single metal−metal bond is symmetric with respect to rotation in the Rh_2 series, rotation about the metal−metal bond will drive the bridging fluorophosphine ligands through an eclipsed conformation. The steric constraints imposed by an eclipsed conformation should result in a significant lengthening of the metal−metal bond and consequently a reduced metal−metal interaction. This in turn should lead to a smaller energy gap and hence more efficient nonradiative decay from an excited state with $d\sigma^*$ character. Indeed, large thermal effects in the absorption and emission spectra of $d\sigma^*$ excited states have been attributed to the large Franck−Condon factors for the thermally accessible metal−metal stretch of dirhenium cores

(19) (a) Milder, S. J.; Brunschwig, B. S. *J. Phys. Chem.* **1992**, *96*, 2189. (b) Lumpkin, R. S.; Kober, E. M.; Worl, L. A.; Murtaza, Z.; Meyer, T. J. *J. Phys. Chem.* **1990**, *94*, 239.

(20) Newman, R. A.; Martin, D. S.; Dallinger, R. F.; Woodruff, W. H.; Stiegman, A. E.; Che, C.-M.; Schaefer, W. P.; Miskowski, V. M.; Gray, H. B. *Inorg. Chem.* **1991**, *30*, 4647.

(21) The calculated energies derived from the spin−orbit matrix places the disallowed state (B or A) below the E state by an amount that is approximately one-half the spin−orbit coupling constant, $1/2\delta$.

(22) The energy gaps of the Pt_2 tetraphosphates reported in ref 8 are in error owing to the use of an incorrect value for the Boltzmann constant in fits of eq 2. The correct values of ΔE for the Pt_2 tetraphosphate series are $\Delta E(K_2Pt_2(HPO_4)_4(H_2O)_2) = 487$ cm^{-1}; $\Delta E(K_4Pt_2(HPO_4)_4Cl_4) = 937$ cm^{-1}; and $\Delta E(K_4Pt_2(HPO_4)_4Br_4) = 856$ cm^{-1}. It should be noted that the rate constants, whose values are not dependent on k_BT in a fit of eqs 1 or 2, are correct in ref 8.

(23) Dauben, W. G.; Salem, L.; Turro, N. J. *Acc. Chem. Res.* **1975**, *8*, 41.

bridged by phosphine ligands.[24] The lowest energy-emitting state of $Re(CO)_6$ $(\overset{\sqcap}{PP})_2$ ($\overset{\sqcap}{PP}$ = bridging phosphine) has been assigned to $^3(\sigma \rightarrow d\sigma^*)$, and the temperature dependence of the emission exhibits a pronounced hot-band effect attributed to the low-excited state $\nu(Re_2)$ vibration. However our observations of a large temperature dependence from microcrystalline samples seem to exclude the possibility of large torsional distortions arising from rotation about the metal−metal bond. Accordingly, as is the case for the $LPt^{III}Pt^{III}L$ tetraphosphates and tetrasulfates, the thermal population of spin−orbit components appears to be the crucial factor controlling the excited state dynamics of the dirhodium fluorophosphine complexes.

Acknowledgment. Financial support of this work by National Science Foundation Grant CHE-9521347 is gratefully acknowledged.

Supporting Information Available: Complete tables of atomic coordinates, bond distances and angles, anisotropic temperature factors, least-squares planes, and torsional angles for **1** and **2** (17 pages). Ordering information is given on any current masthead page.

IC9505615

(24) Milder, S. J.; Castellani, M. P.; Weakley, T. J. R.; Tyler, D. R.; Miskowski, V. M.; Stiegman, A. E. *J. Phys. Chem.* **1990**, *94*, 6599.